Microphysical and radiative properties of tropical clouds investigated in TC4 and NAMMA

R. Paul Lawson,[1] Eric Jensen,[2] David L. Mitchell,[3] Brad Baker,[1] Qixu Mo,[1] and Bryan Pilson[1]

[1] The size, shape and concentration of ice particles in tropical anvil cirrus and in situ cirrus clouds have a significant impact on cloud radiative forcing, and hence on global climate change. Data collected in tropical anvil and cirrus clouds with a 2D-S probe, an optical imaging probe with improved response characteristics and the ability to remove shattered artifacts, are analyzed and discussed. The data were collected with NASA DC-8 and WB-57F research aircraft near Costa Rica during the 2007 Tropical Composition, Cloud and Climate Coupling (TC4) field project, and with the DC-8 near Cape Verde during the 2006 NASA African Monsoon Multidisciplinary Analyses (NAMMA) campaign. Data were collected in convective turrets, anvils still attached to convection, aged anvils detached from convection and cirrus formed in situ. Unusually strong maritime convection was encountered, with peak updrafts of 20 m s^{-1}, ice water contents exceeding 2 g m^{-3} and total particle concentrations exceeding 10 cm^{-3} at 12.2 km. Ice water contents in the anvils declined outward from the center of convection, decreasing to <0.1 g m^{-3} in aged anvil cirrus. The data show that microphysical and radiative properties of both tropical anvils and cirrus are most strongly influenced by ice particles in the size range from about 100 to 400 μm. This is contrary to several previous investigations that have suggested that ice particles less than about 50 μm control radiative properties in anvils and cirrus. The 2D-S particle area and mass size distributions, plus information on particle shape, are input into an optical properties routine that computes cloud extinction, asymmetry parameter and single scattering albedo. These optical properties are then input into two-stream radiative code to compute radiative heating profiles within the various cloud types. The results produce short- and long-wave heating/cooling vertical profiles in these tropical clouds. A simple parameterization based on 2D-S measurements is derived from the particle mass size distribution that yields an area size distribution. The parameterized area size distribution can then be used in large-scale numerical simulations that include radiative transfer packages.

Citation: Lawson, R. P., E. Jensen, D. L. Mitchell, B. Baker, Q. Mo, and B. Pilson (2010), Microphysical and radiative properties of tropical clouds investigated in TC4 and NAMMA, *J. Geophys. Res.*, *115*, D00J08, doi:10.1029/2009JD013017.

1. Introduction

[2] The size, shape and concentration of ice particles in anvil cirrus and in situ cirrus clouds have a significant impact on cloud radiative forcing, and hence global climate change. *Stephens et al.* [1990] and others have shown that shape is an important factor that affects how much short wave radiation reaches the surface of the Earth. Remote retrievals of ice water content depend on a priori assumptions about the shape of ice crystal size distributions. *Mishchenko et al.* [1996] found that using the wrong particle

shape can produce an error of a factor of three in cloud optical depth. Ice crystal size strongly influences the balance between cirrus longwave and solar shortwave cloud radiative forcing [*Stackhouse and Stephens*, 1991; *Jensen et al.*, 1994]. *Jensen et al.* [2009] show that the concentration of small ice particles has often been overestimated in previous papers due to large ice crystals shattering on probe inlets, and that this has likely introduced significant errors in anvil cirrus cloud extinction and radiative heating profiles.

[3] *Sinha and Shine* [1994] show that including the small-crystal mode in parameterized size distributions affects cirrus cloud/climate feedback. *Sanderson et al.* [2008] used an ensemble of thousands of general circulation model (GCM) simulations and found that ice crystal fall speed, which is a function of crystal size assumed in the cirrus parameterizations, was a major factor that influenced climate variation. *Mitchell et al.* [2008] showed in GCM simulations that

[1]SPEC, Incorporated, Boulder, Colorado, USA.
[2]NASA Ames Research Center, Moffett Field, California, USA.
[3]Desert Research Institute, University of Nevada, Reno, Nevada, USA.

cirrus ice mass, cirrus coverage, and cloud radiative forcing are very sensitive to assumptions about the concentration of small (diameter <60 μm) crystals in the cirrus parameterization.

[4] The Tropical Composition, Cloud, and Climate Coupling (TC4) is the first major, multi-aircraft, comprehensive investigation of Tropical anvil clouds [*Toon et al.*, 2010]. Previously, *Griffith et al.* [1980] collected measurements with a Particle Measuring Systems (PMS) 1-D optical array probe (nominally 20 to 300 μm) installed on a Sabreliner in tropical anvils. They found that the ice water content (IWC) ranged up to a few tenths g m^{-3} and decreased toward cloud top. *Knollenberg et al.* [1982, 1993] investigated tropical anvils between 13 and 18 km using PMS scattering and 1-D imaging probes installed on the NASA ER-2 research aircraft. They report IWC values <0.1 g m^{-3} of small (<100 μm) ice crystals in high (>1 cm^{-3}) concentrations near cloud tops at −90°C. The most extensive in situ measurements of Tropical anvils prior to TC4 was the Central Equatorial Pacific EXperiment (CEPEX), which was conducted near Fifi using a Learjet model 36 research aircraft. *McFarquhar and Heymsfield* [1996] report results from 150 km horizontal legs at altitudes ranging from about 9.8 km (−20°C) to 13.9 km (−60°C). The instrumentation consisted of PMS 2D cloud and precipitation optical array probes [*Knollenberg*, 1981], PMS FSSP-300 [*Baumgardner et al.*, 1992] and a video ice particle sampler [*McFarquhar and Heymsfield*, 1996]. Particle concentrations measured by the 2D probes did not exceed a few hundreds per liter and derived IWC values were <0.3 g m^{-3}. FSSP-300 particle concentrations exceeded 1 cm^{-3}, but McFarquhar and Heymsfield wisely questioned these measurements in ice crystals and did not include them in their determination of total particle concentration. They report that small (<100 μm) ice crystals made substantial, but variable contributions to IWC and extinction near cloud top where IWC values were typically a few hundredths g m^{-3}. They concluded that the radiative properties of large crystals near the anvil base were as important as the small crystals at cloud top in determining radiative properties of thick anvils. Recent analysis of the time response of the 2D probes used on the CEPEX Learjet show that they were incapable of reliably measuring particles with sizes smaller than about 150 μm at Learjet airspeeds [*Lawson et al.*, 2006a], and that the smaller particle images were actually larger particles that were incorrectly sized.

[5] Data were collected during TC4 and the NASA African Monsoon Multidisciplinary Analyses (NAMMA) campaign with a 2D-S probe, an optical imaging probe with improved response characteristics capable of measuring 10 μm particles at jet airspeeds, and the ability to remove shattered artifacts [*Lawson et al.*, 2006a; *Baker et al.*, 2009a, 2009b]. Using 2D-S data from TC4, *Jensen et al.* [2009] argue that, compared with the large ice mode, small ice crystals (less than about 60 μm) rarely make a significant contribution to cloud extinction and optical depth in deep tropical cirrus anvils. These results are contrary to reports that suggest that small ice may play a dominant role in the radiative properties of cirrus anvils [e.g., *Knollenberg et al.*, 1993; *Kärcher and Ström*, 2003; *Garrett et al.*, 2003, 2005; *Fridlind et al.*, 2004; *Davis et al.*, 2009].

[6] This paper extends the analysis of CEPEX tropical anvil data reported by *McFarquhar and Heymsfield* [1996],

and TC4 anvil data analyzed by *Jensen et al.* [2009]. We examine the microphysical and radiative properties of tropical cirrus and cirrus anvils from NASA field programs conducted off the west coast of Costa Rica (TC4) and the west coast of Senegal (NAMMA). The TC4 field project was staged from San Jose, Costa Rica in August 2007 and the NAMMA field campaign was based on the Cape Verde Islands and Senegal in August–September 2006. Microphysical and radiative products based on data collected within in situ cirrus (cirrus formed from vertical lifting in the upper troposphere), in fresh and aged anvil cirrus (formed via deep convection), and in convective updrafts from both TC4 and NAMMA are discussed and compared.

2. Data Collection

2.1. TC4 and NAMMA Field Campaigns

[7] The TC4 field campaign focused on clouds, chemistry and composition of the upper tropical troposphere [*Toon et al.*, 2010]. The DC-8 spent a large majority of its flight hours investigating 1) the upper portions of fresh anvil cirrus, 2) deep aged anvil cirrus, 3) in situ cirrus and 4) limited penetrations of vigorous embedded convective turrets. Figure 1 shows satellite visual images that contain examples of these four cloud types. Table 1 lists the days, times, flight altitudes and temperatures of DC-8 legs flown in four cloud types during both the TC4 and NAMMA field campaigns. Due to technical limitations, the NASA WB-57F research aircraft was only available for the first week in August 2007. Minimal measurements from the WB-57F are included in this paper in order to show data in thin cloud above the DC-8 maximum altitude of 12.2 km (FL 400). (Aircraft typically fly at increments of 1,000 ft (305 m). In this paper we include the aviation FL convention, where FL × 100 = altitude in thousands of ft.)

[8] Fresh anvil cirrus is cloud that is still attached to its parent convection. The DC-8 flew extensively in cirrus anvils and occasionally penetrated active convection. The results described in this paper include DC-8 data collected in fresh anvil cirrus from 9.2 km (FL300) up to and including 11.3 km (FL370). Some results from penetrations in convective turrets, which were the source for ice crystals observed in the anvils, are presented here for comparison purposes.

[9] We define aged anvil cirrus as cloud that has disconnected from its parent convection and has existed for about 2 to 3 hours. The aged anvil cloud systems were often deep, extending from about 12.2 km (FL400), and occasionally higher, down to about 5.5 km (FL180). These systems may have extended lower and even developed rain at the surface, but this lower region of the cloud system was not investigated. The DC-8 conducted profiles from 12.2 km (FL400) down to 7.3 km (FL240) in aged anvil cirrus. The WB-57F added measurements from 14.6 km (FL480) to 12.8 km (FL420) during a coordinated investigation of aged anvil cirrus on 5 August 2007.

[10] In situ cirrus, formed via vertical lifting in the upper troposphere, and generally about 1 km thick, was encountered at altitudes between 9.8 km (FL320) and 11.3 km (FL 370). In situ cirrus was easily identified because it often contained ice crystals that were bullet rosette shaped. *Lawson et al.* [2006b] analyzed CPI images from 104 aircraft horizontal

Table 1. Summary of Data Analyzed in TC4 and NAMMA Clouds

Projects and Cloud Type	Time in Cloud	Flight Levels	Temperatures
TC4 Turrets	2.35 min	FL300–FL380	−32 C to −54 C
NAMMA Turrets	37 min	1,200 ft–FL370	+23 C to −49 C
TC4 Anvils	48 min	FL270–FL370	−24 C to −51 C
NAMMA Anvils	117 min	FL280–FL340	−25 C to −40 C
TC4 Aged Cirrus	243 min	FL300–FL480	−31 C to −69 C
TC4 In Situ Cirrus	119 min	FL380–FL400	−54 C to −58 C
NAMMA In Situ Cirrus	41 min	FL320–FL370	−34 C to −51 C

legs in cirrus between −30 and −61°C and found that more than 40% of the ice particles >50 μm were rosette shaped. Fresh anvil clouds rarely contained bullet rosette shapes, and instead were composed mostly of irregular shapes, plates, columns and aggregates. Particle shapes in aged cirrus were similar to fresh anvil cirrus, but sometimes contained rosette shapes, suggestive of newly nucleated ice particles.

[11] Figure 2 shows examples of 2D-S images and some CPI images typically observed in the four types of TC4 cloud systems described in this paper. Due to the location of the CPI close to the fuselage of the DC-8 it did not see particles larger than about 300 μm. Also included in Figure 2 are particle images from the WB-57 at 11km (FL360), 113.4 km (FL440) and 14.6 km (FL480) collected on 8 August 2007 in aged cirrus.

[12] The NAMMA field campaign was designed to follow mesoscale cloud systems that form over or near West Africa. These cloud systems sometimes evolve into hurricanes that are eventually advected over the eastern Atlantic, and sometimes strike Central or North America [*Vizy and Cook*, 2009]. The DC-8 encountered several different cloud systems during NAMMA, some of which were similar to those investigated in TC4. In particular, fresh cirrus anvils, convective turrets and in situ cirrus were investigated. Aged anvil cirrus likely existed but was not a target during NAMMA and therefore was not investigated. Figure 3 shows examples of satellite visual images of NAMMA cloud systems. Figure 4 shows particle shapes observed in fresh anvil cirrus, convective turrets and in situ cirrus during NAMMA. Data from both TC4 and NAMMA cloud systems that are presented in this paper are characteristic of convection that occurs within or very near the inter-tropical convergence zone (ITCZ) in each region.

2.2. Instrumentation

[13] The NASA DC-8 and WB-57 research aircraft typically fly in cirrus anvils at true airspeeds of about 225 and 190 m s^{-1}, respectively. Other optical cloud particle probes were installed on the NASA aircraft, including cloud imaging probes (CIP) and a cloud and aerosol spectrometer (CAS) probe [*Baumgardner et al.*, 2001]. Investigations reported in the literature have shown good general agreement between the 2D-S and CIP size distributions for particles larger than about 300 μm [e.g., *Jensen et al.*, 2009; A. V. Korolev et al., Small ice particles in tropospheric clouds: Facts or artifacts? Airborne Icing Instrumentation Evaluation Experiment, submitted to *Bulletin of the American Meteorological Society*, 2010]. However, for smaller particles the CIP probe does not appear to have sufficient time response to reliably image particles at the typical airspeeds of the WB-57F and DC-8. This is demonstrated on Figure 5, which shows a comparison of CAS, CIP and 2D-S size distributions recorded by the WB-57F at true airspeeds ranging from 175 to 195 m s^{-1}. The data were collected in regions where the maximum particle size, determined from in-focus CPI and 2D-S images, was limited to approximately 150, 200 and 250 μm, respectively. *Tian et al.* [2010] compared CIP and 2D-S TC4 data and chose to limit their analysis of CIP data to images >100 μm. The 2D-S probe has demonstrated in the laboratory the ability to accurately size particles as small as 8 μm at an equivalent airspeed of 233 m s^{-1} [*Lawson et al.*, 2006a]. This is unique
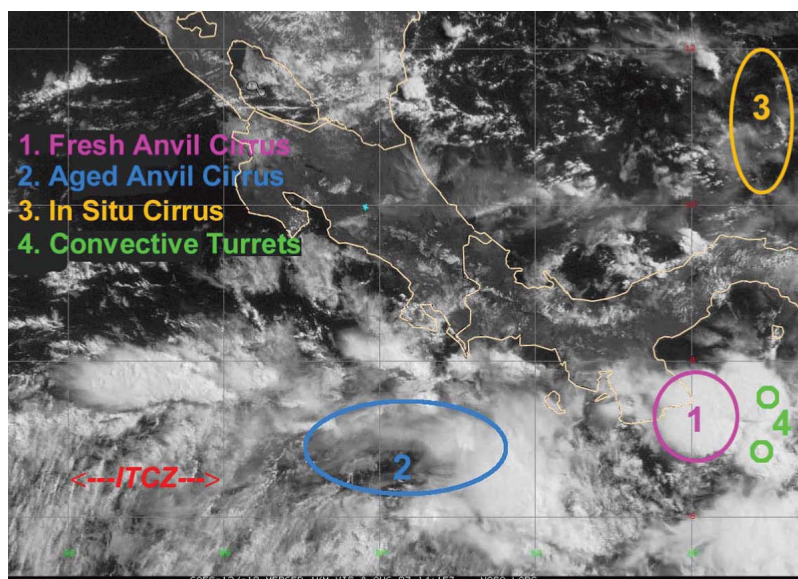
Figure 1. Goes-12 satellite visual image on 8 August 2007 at 14:15 UTC showing examples of cloud types observed during the TC4 project and discussed in this paper.
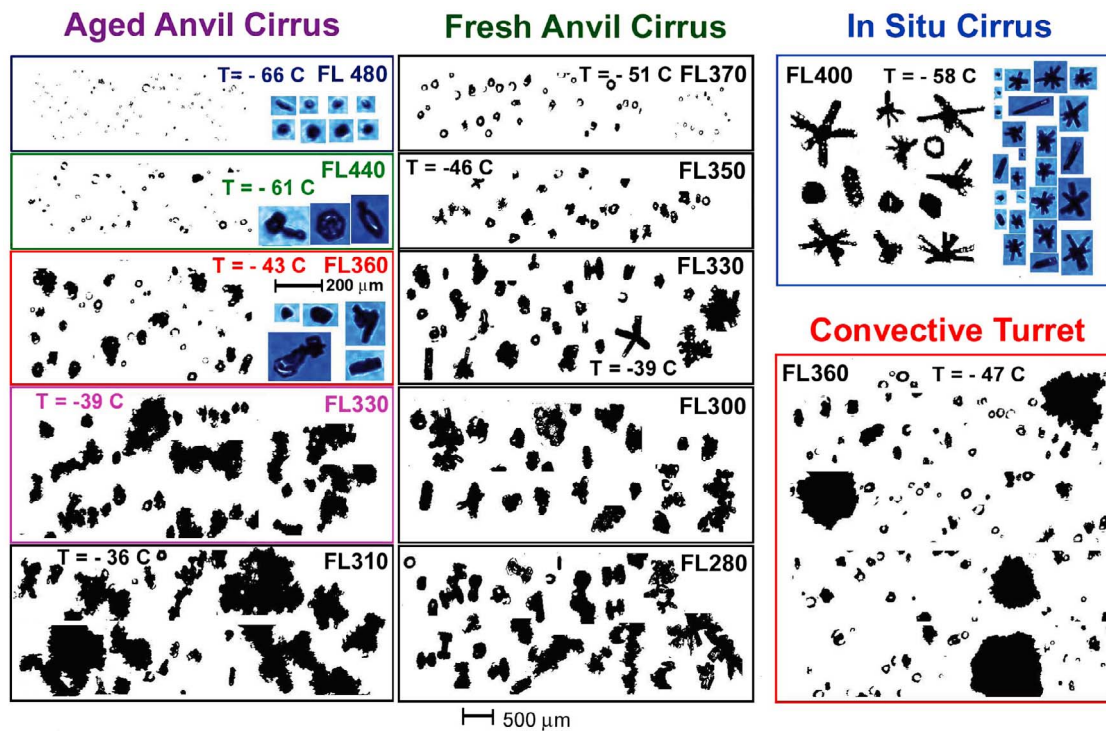
Figure 2. Examples of particle images from TC4. The data from 14.6 km (FL480), 13.4 km (FL440) and 11 km (FL360) are from the NASA WB-57 aircraft. All other images were collected by the DC-8.

among (linear photodiode array) optical imaging probes and is one reason these data are being used in this study. A second reason is that individual particle arrival times are recorded and used to reject small ice artifacts resulting from large ice shattering on the probe tips. Using particle arrival time to reject shattered cloud particle artifacts is not new [i.e., *Cooper*, 1978], but has received renewed attention in the more recent literature [e.g., *Field et al.*, 2003; *Korolev and Isaac*, 2005; *Field et al.*, 2006; *Baker et al.*, 2009a, 2009b]. It is important to note that when the true small particle concentration is very low compared to the effect of shattering, the resulting estimate of small particle concentration (after removing shattering) has an uncertainty as large as the estimate itself. That is, when the natural small ice concentration is very low and the mass of large ice is high, producing many small shattered particles, the remaining small images may still be dominated by shattering. Thus, it is best to consider the estimate, in these cases, as an upper bound of the possible small particle concentration. As will be seen in later sections, the percentage of small ice particles removed via the 2D-S shattering algorithm in the cloud regions reported here were a small fraction of the remaining small ice concentration.

[14] The 2D-S probe was processed using individual particle inter-arrival times to minimize the effects of large ice particles shattering on the probe tips. *Jensen et al.* [2009] show examples of 2D-S particle size distributions (PSDs) with and without the effects of shattering, along with comparisons to PSDs from the CAS probe, which *Heymsfield* [2007] *Jensen et al.* [2009] have shown is effected by shattering. *Jensen et al.* [2009] suggest that, when compared with 2D-S measurements in some cloud regions examined in

TC4, shattering on the CAS produces a very large overestimate in particle concentration. Figure 5 shows that, compared with the 2D-S, shattering on CAS probe increases with increasing particle size. The TC4 data show that shattering on the CAS has the largest relative impact on measured ice
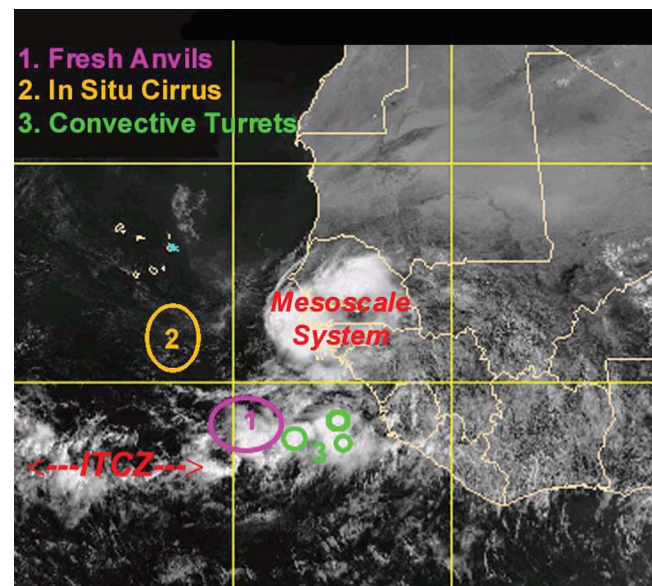
Figure 3. Goes-12 satellite visual image on 11 September 2006 at 1515 UTC showing examples of cloud types observed during the NAMMA project and discussed in this paper.
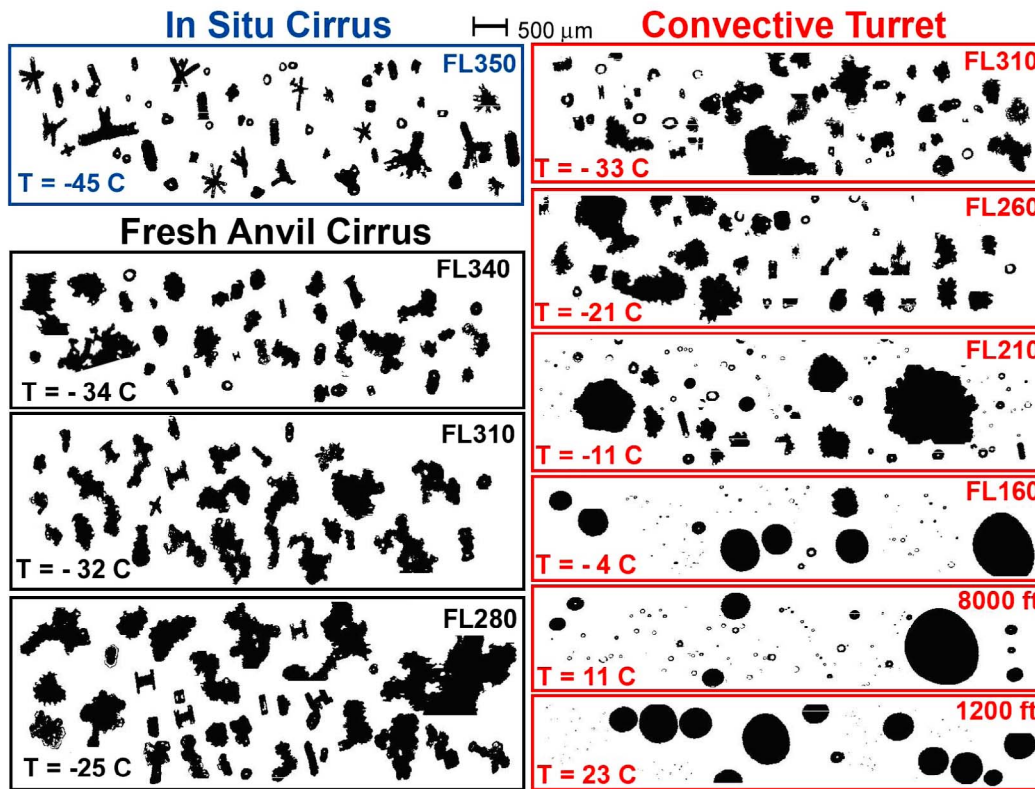
Figure 4. Example of 2D-S particle images collected in various cloud types by the DC-8 during NAMMA.

concentration when there are high concentrations of large ice and low concentrations of small ice [*Jensen et al.*, 2009].

[15] There is no standard that can be used to quantitatively evaluate parameters derived from 2D optical imaging probes (e.g., particle concentration, extinction coefficient and IWC). Some investigators have provided estimates of derived parameters in previous publications, but unfortunately, it is often subsequently learned that significant instrumentation errors (such as inadequate time response and ice crystals shattering on probe tips) severely biased the estimates. Since in situ measurements are often considered "ground truth", remote retrievals and numerical models are sometimes tuned

to agree with the in situ values, and optimistic error bars are propagated through to the retrievals and models.

[16] In lieu of presenting error bars for derived parameters, we elect instead to show a comparison of a derived parameter, IWC, which can be compared with another instrument that has a totally different measurement technique. We follow the approach presented by *Heymsfield* [2007] and compare the IWC derived from two-dimensional images with a device that measures mass in a more direct manner, in this case the counterflow virtual impactor (CVI) [*Twohy et al.*, 1997]. Using this approach, we derive a correlation coefficient between 2D-S and CVI IWC, but we
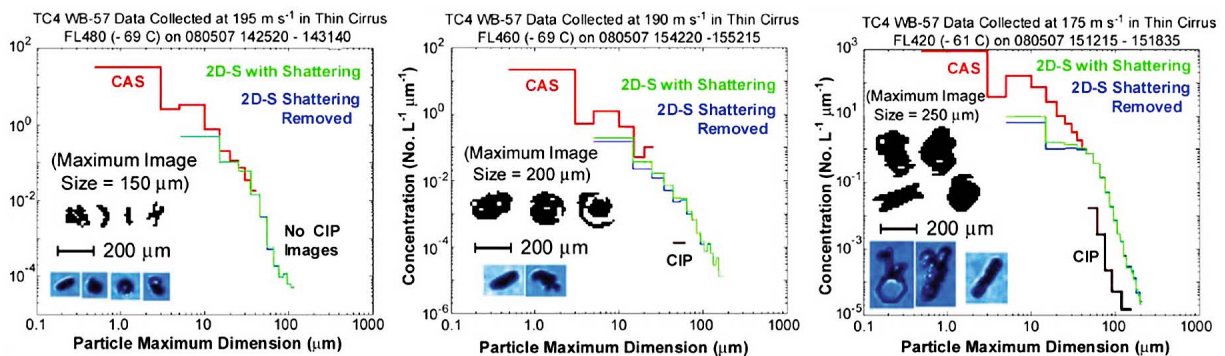
Figure 5. Particle size distributions comparing 2D-S, CAS and CIP WB-57F measurements in thin cirrus with maximum particle size of (left) 150 μm, (middle) 200 μm and (right) 250 μm. See text for further explanation.
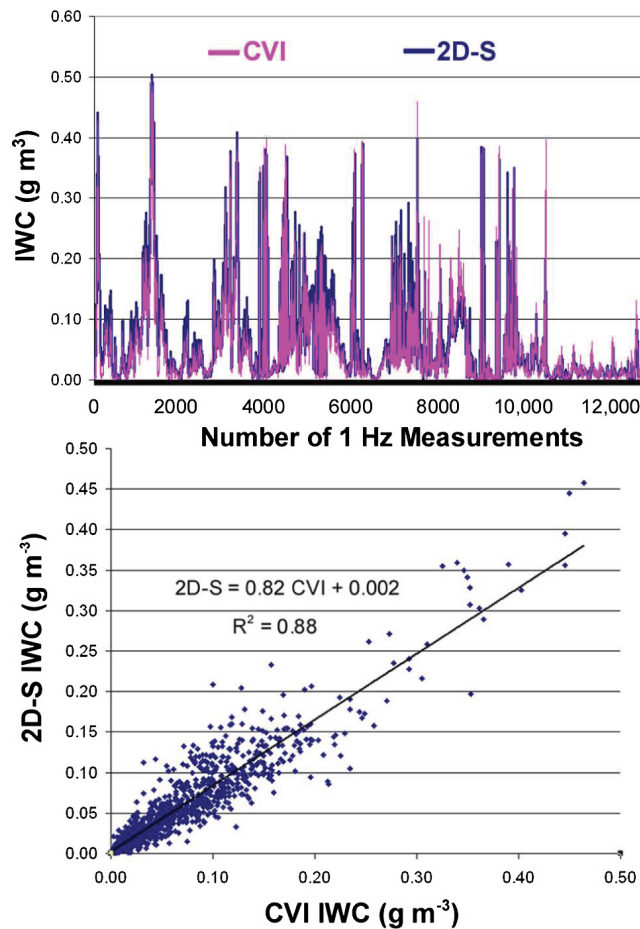
Figure 6. (top) Time series of 1-Hz IWC measurements from CVI and 2D-S. The 12,000 measurements are combined from two days (22 July and 8 August, 2007) when the DC-8 sampled fresh anvil cirrus (i.e. anvil still connected to convection), aged anvil cirrus (i.e., anvil disconnected from convection and existing for 2 to 3 hours) and cirrus formed in situ. CVI measurements have been processed to remove hysteresis by zeroing CVI IWC when 2D-S (and other particle probes) did not detect any particles. (bottom) Scatterplot of 10-s averaged measurements shown above in the time series.

do not propagate this approach into error bars, because the CVI itself cannot be compared with a IWC standard in an airborne configuration.

[17] Figure 6 shows a comparison of IWC from the CVI installed on the NASA DC-8 during TC4 and IWC derived from 2D-S particle imagery. 2D-S IWC was computed from 2D-S images using the area-to-mass relationship from *Baker and Lawson* [2006a]. The data in Figure 6 were collected on 22 and 24 July, 5 and 8 August in 1) fresh anvil cirrus that was still connected to convection, 2) aged anvil cirrus that was disconnected from convection and had existed for 2 to 3 hours, and 3) thin cirrus that formed in situ. The data regions were selected so that the comparison included several different particle types (Figure 2) and a range of IWC values. The comparison is limited to IWC's of 0.5 g m^{-3} because the CVI usually saturated at higher

values. (The CVI saturation threshold varies directly with increasing flow rate, which can be adjusted by the operator. During TC4 the flow rate was often set to a relatively low value to accommodate other mission priorities.)

[18] We use 2D-S data to derive PSDs, values of particle concentration, extinction coefficient and IWC that are typical of the three cloud systems. Extinction is computed by multiplying twice the projected area of each 2D-S particle image by 0.75. The 2D-S data appear to be a reliable estimate of these parameters, and represent the first comprehensive data set that can be used to compute radiative forcing in these cloud systems. We use 2D-S PSDs that are a function of area and mass, as well as particle shape recipes, as inputs to codes that compute optical [*Mitchell*, 2000, 2002; *Mitchell et al.*, 1996, 2006] and radiative [*Toon et al.*, 1989] properties.

3. Microphysics

3.1. In Situ Cirrus

[19] In situ cirrus are clouds that have formed from vertical lifting in the upper troposphere, in contrast to anvil cirrus that contain particles formed in deep convective updrafts. Table 2a shows a comparison of in situ cirrus bulk properties and particle habits from TC4, NAMMA and mid-latitude cirrus. *Lawson et al.* [2006b] describes the mid-latitude cirrus study, which investigated cirrus formed in situ and measured small particles using a forward scattering spectrometer probe (FSSP). *Field et al.* [2003] have shown that FSSP measurements of small ice in the presence of large ice are often contaminated with shattered artifacts. Therefore, the number concentrations of small particles in the mid-latitude study are likely to be over estimated. Satellite photos in Figures 1 and 3 reveal the relatively low optical depth of in situ cirrus compared with anvil cirrus. The satellite observations qualitatively confirm that relatively low values of extinction coefficient shown in Table 2a. In situ cirrus, other than those clouds associated with deep synoptic or orographic systems, are generally on the order of 0.5 to 2 km thick. The values in Table 2a are averages over all legs at the same altitude. Using these average values results in a typical optical depth of tropical in situ cirrus from about 0.25 to 2. Table 2b and the particle images in Figures 2 and 4 also show that irregular-shaped particles (i.e., shapes that cannot be identified as resembling a specific habit) are the dominant shapes in both Tropical and Mid-latitude cirrus. It is not unusual to find a predominance of irregular shaped particles in ice clouds. *Korolev et al.* [1999] analyzed about 1 million CPI images in ice clouds and found

Table 2a. Average Bulk Properties of in Situ Cirrus Investigated on 22 July During TC4 and 19 and 26 August, and 3 September 2006 During NAMMA, and Midlatitude Cirrus Reported by *Lawson et al.* [2006b][a]

Cloud Type	Concentration (Number per L)	Extinction (km^{-1})	IWC (g m^{-3})
TC4 In Situ Cirrus	198	0.50	0.011
NAMMA In Situ Cirrus	37.0	0.67	0.019
Mid Latitude Cirrus	846	0.46	0.005

[a]Temperature ranged from −45 to −58°C for the TC4 and NAMMA measurements, and −50 to −63°C for the midlatitude measurements.

Table 2b. Particle Shapes for TC4 and NAMMA Clouds and the Midlatitude Investigations[a]

Habit Classifications (%)	Spheroids	Columns	Plates	Irregulars	Rosettes
Tropical In Situ Cirrus	8	5	2	51	34
Mid Latitude Cirrus	3	3	2	63	29

[a]Temperature ranged from −45 to −58°C for the TC4 and NAMMA measurements, and −50 to −63°C for the midlatitude measurements.

that over 95% could not be classified as pristine. However, when crystal habits are recognizable in both Tropical and Mid-latitude cirrus formed in situ, the rosette shape is typically observed (see *Lawson et al.* [2006b] and Table 2b), along with other crystal habits.

[20] Rosette shapes (polycrystals) form at cold (<~−30°C) temperatures when a water drop or solution drop freezes and forms multiple growth sites, or facets. The result is a rosette shape with "arms" protruding from a central point. The presence of rosette shapes is a distinguishing feature of ice that has nucleated and grown at cold temperature, compared with ice that nucleates and grows at lower (warmer) altitudes in convective updrafts. Small ice particles that form via homogeneous freezing of cloud drops (T = −37°C) in an updraft should also be candidates for development into ice with rosette shapes, i.e., small drops that freeze homogeneously should form rosette shapes if they continue to grow in an anvil. However, rosette shapes were rarely observed in TC4 and NAMMA anvils, nor have they been observed with any frequency in fresh anvils in other locations [e.g., *Connolly et al.*, 2005], suggesting that typically conditions are not favorable for growth of these small particles in anvils. However, a small percentage of rosette shapes are found in aged anvil cirrus discussed in the next section, and have also been observed in anvils hundreds of km downwind from convection near Darwin [*Connolly et al.*, 2005], suggesting that subsequent development is possible when anvil cloud is advected into a favorable growth regime (i.e., supersaturated with respect to ice).

[21] The average total ice particle concentrations in the in situ cirrus clouds investigated during TC4 and NAMMA are considerably lower than the average mid-latitude cirrus values reported by *Lawson et al.* [2006b] in Table 2a, and also lower than reported by other investigations in Mid-latitude cirrus [e.g., *Gayet et al.*, 2002; *Kärcher and Ström*, 2003]. However, the formation process of TC4 and NAMMA cirrus may be different than the cirrus formed in Mid-latitudes. Also, unlike the present measurements, the previous studies mentioned above relied mostly on FSSP measurements (and CVI in the Kärcher and Ström investigation), which have been shown to overestimate the actual concentration due to shattering of large ice particles on the probe inlet [*Field et al.*, 2003; *Jensen et al.*, 2009]. Even though the number concentrations shown in Table 2a are significantly higher in Mid-latitude cirrus than in Tropical cirrus, values of extinction and IWC are comparable, suggesting that the second and third moments may be influenced more by particles that are larger than the shattered artifacts.

[22] Figure 7 shows average PSDs as a function of particle concentration, area and IWC from TC4 and NAMMA in situ cirrus. The PSDs from the two sites contain some differences. For example, there are fewer smaller particles and higher concentrations of larger particles in NAMMA than in

TC4, but overall they are quite similar, especially when compared with PSDs in anvil cirrus that is discussed in the next section. The most noticeable feature in Figure 7 is that the area and mass size distributions are dominated by particles from about 100 to 400 μm. That is, as shown in Figure 7b, there is about twice as much area in particles from 100 to 400 μm than there is from 400 to 3,000 μm, and about 5 times as much area than there is in particles from 10 to 100 μm. A similar relationship is seen in the IWC PSD (Figure 7c). As we shall see in the next section, this same trend holds for cirrus anvils and convective turrets.

3.2. Anvils

[23] Fresh anvil cirrus are analyzed from data collected on 22 and 24 July 2007 during TC4, and from 19, 20, 25 August and 1 September 2006 during NAMMA. The DC-8 flew 1,000 ft increments from 9.2 km (FL300) up to and including 11.3 km (FL 370). Vigorous convective turrets were investigated on 22 and 24 July at 12.2 km (FL400) during TC4, and from 5.8 km (FL190) to 11.3 km (FL370) on 19 and 20 August 2006 during NAMMA. Results from aged anvil cirrus are presented from TC4 data collected on 5 and 8 August 2007. Aged anvil cirrus was not a target in NAMMA.

[24] Figure 8 shows examples of PSDs and Table 3 contains bulk parameters derived from the particle concentration, area and IWC PSDs for convective turrets, fresh anvil
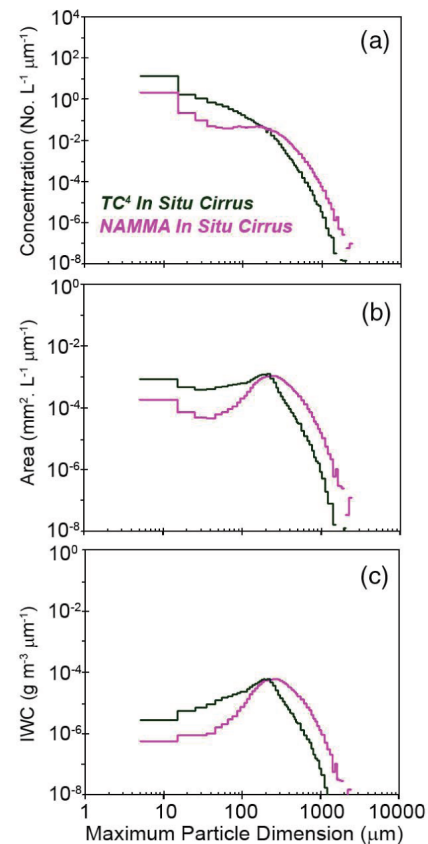
Figure 7. Averaged particle size distributions as a function of particle (a) concentration, (b) area and (c) mass derived from 2D-S measurements collected by the DC-8 in cirrus formed in situ.
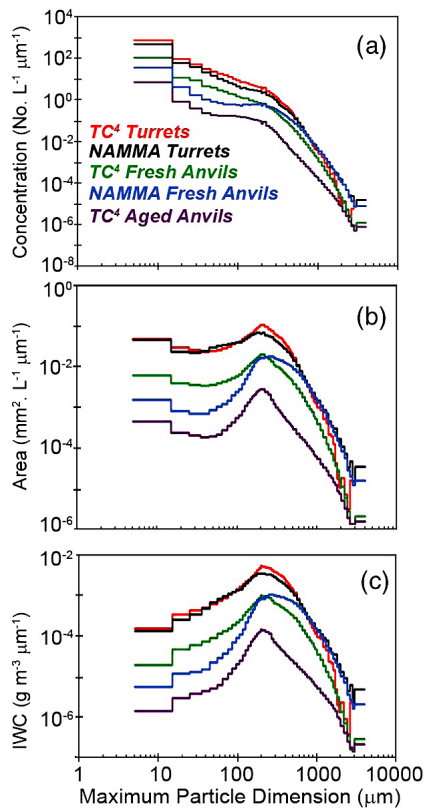
Figure 8. Averaged particle size distributions as a function of particle (a) concentration, (b) area and (c) mass derived from 2D-S measurements collected in convective turrets, fresh anvil cirrus and aged anvil cirrus by the DC-8 in TC4 and NAMMA.

cirrus and aged anvil cirrus. The values of all three moments of the particle size distribution in Table 3 vary in an expected manner; the turrets have the highest values, followed by the fresh anvil cirrus and finally the aged anvil cirrus. This is expected due to the following processes. The particles in the turrets are relatively large (>1 mm) and also contain the highest concentration of small particles due to the strong, sustained updraft, which is responsible for particle formation and growth. The particles in the anvil come from the turrets, after spreading out over a larger area and entraining environmental air. During this process, some of the small particles are likely to sublimate and some larger particles sediment out of the anvil. This scenario assumes there is no subsequent particle growth in the fresh and aged anvils. This is generally a valid assumption, since (polycrystalline) rosette shapes are often observed at these cold temperatures [*Lawson et al.*, 2006b; *Baker and Lawson*, 2006b], and rosette shapes were observed only in sparse concentrations in TC4 and NAMMA anvils (Figures 2 and 4).

[25] The PSDs in Figures 7 and 8 are mostly consistent with the bulk parameters in Tables 2 and 3. With some minor exceptions, there are fewer particles at all sizes in fresh anvils compared to turrets, in aged anvils compared with fresh anvils. The Tropical average in situ cirrus particle concentration ranges from 37 to 198 L^{-1}, which brackets the average particle concentration (114 L^{-1}) in aged anvil cirrus. The most notable feature in Figure 8 is that, like the Tropical

in situ cirrus (Figure 7), the particles in the 100 to 400 μm size range in cirrus anvils and convective turrets provide the dominant contribution to extinction and IWC. The physics behind these consistent observations may be due to a combination of factors, as suggested in the following scenario. In the strong turrets, a few water drops nucleate early and freeze at warmer temperatures (T > −10°C), growing via vapor diffusion to sizes where they reach the riming threshold, which depending on crystal type is typically about 150 to 300 μm [see *Baker and Lawson*, 2006b]. These crystals grow rapidly via accretion in the high LWC environment and quickly become small graupel particles, as seen at 6.4 km (FL210) in Figure 4. The graupel particles are initially carried upwards and continue to grow until they eventually fall down through the updraft. Only traces of LWC were observed in NAMMA clouds at temperatures colder than −12°C, which is consistent with observations in clouds observed near Kwajalein by *Stith et al.* [2002]. Thus, the remaining cloud drops may nucleate heterogeneously at colder temperatures (T < −12°C) in the updraft, but there is not sufficient water vapor pressure for them to grow much larger than a few hundreds of microns. The low LWC in the colder regions of the updraft favors aggregation of these crystals, instead of formation of graupel [*Cooper and Lawson*, 1984]. Aggregation accounts for the larger end of the size distribution in the upper portion of the updraft, as seen images at 8 m (FL260) and 9.5 km (FL310) in Figure 4, except when the updraft velocity is extremely strong and graupel particles are lofted to these higher elevations. Eventually, all of the cloud drops in the updraft freeze homogeneously when they reach −40°C.

[26] Based on this scenario, the anvil is thus supplied with a low concentration of large aggregates, a moderate concentration of intermediate size crystals that grew mostly by vapor diffusion and some riming, and small quasi−spheroidal particles that nucleated homogeneously. As the anvil spreads out downwind and ages, the small quasi-spheroidal particles sublimate and/or aggregate, the large aggregates sediment out and the intermediate sized particles remain until they form aggregates lower in the anvil. This process is exemplified in Figure 9 that shows data from a series of passes at various altitudes through TC4 anvils sampled by the DC-8 on 22 July 2007. At progressively lower altitudes the particles in the size range from 20 to 400 μm are systematically depleted, while the concentration of particles >400 μm does not change significantly. We postulate that this is because smaller particles are aggregating into larger particles while the largest particles continue to fall out of the anvil. The smallest particles could be either sublimating or consumed in the aggregation process.

Table 3. Average Properties of Particle Concentration, Extinction Coefficient, and IWC Derived From 2D-S Data for Various Cloud Types Investigated by the DC-8 in TC4 and NAMMA

| Cloud Type	Concentration (Number per L)	Extinction (km^{-1})	IWC ($g\ m^{-3}$)
TC4 Turrets	11100	60.0	1.65
NAMMA Turrets	7120	48.1	1.36
Fresh TC4 Anvils	1540	11.0	0.32
Fresh NAMMA Anvils	630	16.4	0.56
TC4 Aged Anvil Cirrus	114	1.24	0.036
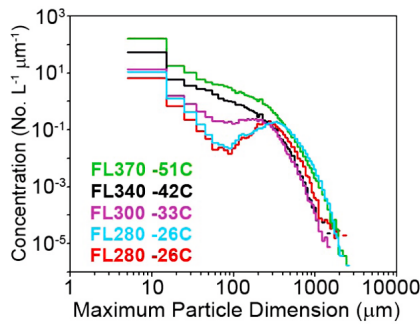
Figure 9. Particle size distributions averaged over horizontal penetrations of a convective turret investigated during NAMMA on 20 August 2006.

[27] As shown in Table 3, anvil cirrus that is still attached to active convection has values of particle concentration, volumetric extinction coefficient and IWC that are lower than found in the turrets and higher than those in aged anvil cirrus that has detached from convection. As expected, the values of number concentration, extinction and IWC all decrease with increasing distance from convection that generates the anvil. This trend is shown in Figure 10, which is based on data collected at 11.3 (FL370) on 24 July 2007 when the DC-8 flew from the anvil edge inward to the center of convection. The three distinct humps in the time series of each trace are likely the result of convective pulses from individual turrets. The trend of mass concentration decreasing outward from the location of convection was also reported by *McFarquhar and Heymsfield* [1996] in Tropical anvils, and by *Lawson et al.* [1998a] in Tropical and Mid-latitude anvils. The decrease in total particle concentration is

due to spreading of the anvil, sublimation and/or aggregation of the smaller particles, and sedimentation of the larger particles. Although the CPI imagery was limited to particles smaller than about 300 μm, there was no suggestion of aggregates of chains of small particles, such as found by *Connolly et al.* [2005] in continental anvils that typically have higher electric fields than maritime anvils.

[28] Aged anvil cirrus has detached from its parent convection. Generally, as shown in Figure 8 and Table 3, aged anvil cirrus contains about an order of magnitude fewer particles of all sizes, with the maximum particle size decreasing from a few millimeters to about one millimeter. This suggests that the cloud is being diluted as it spreads and depleted by sublimation and sedimentation at a much faster rate than any replenishment due to particle nucleation and growth. As expected, particle sorting due to sedimentation and aggregation results in the smallest particles near cloud top and the largest particles near cloud base (Figure 2). Figure 11 shows particle size distributions of concentration, area and mass, and mean bulk properties averaged over horizontal legs during the combined WB-57F/DC-8 investigation of aged cirrus on 5 August 2007. The data in Figure 11 show that small particles only make a significant contribution to extinction and IWC in the very thin cloud near cloud top, in this case from 12.8 km (FL420) to 14.6 km (FL480). Bulk properties are computed from the average particle size distributions. Effective radius (R_{eff}) is computed by multiplying particle volume (using the area-to-volume relationship from *Baker and Lawson* [2006a]) by 0.75 and dividing by particle projected area. R_{eff} and extinction coefficient (β_{ext}) decrease from 18.7 μm and 0.14 km^{-1} to 5.8 μm and 0.005 km^{-1} between 12.8 km (FL420) and 14.6 km (FL480). In the region from 9.2 km (FL300) to 11.3 km (FL370), R_{eff}
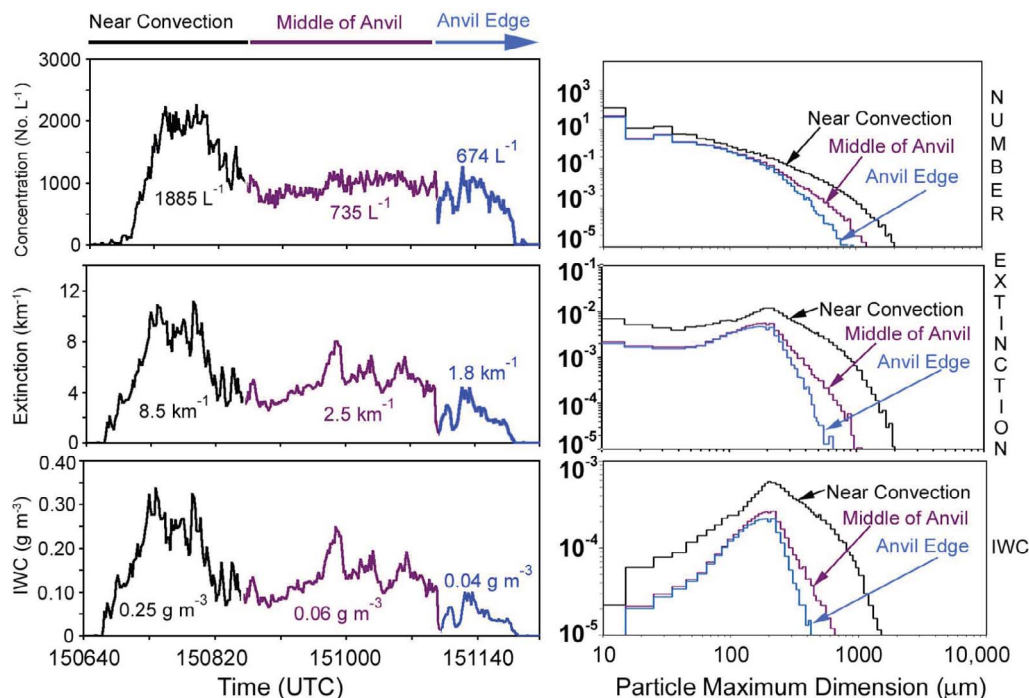
Figure 10. (left) Time series and (right) particle size distributions as a function of (top) concentration, (middle) extinction and (bottom) IWC for transect of an anvil on 24 July that proceeded from near the center of convection to the edge of the anvil.
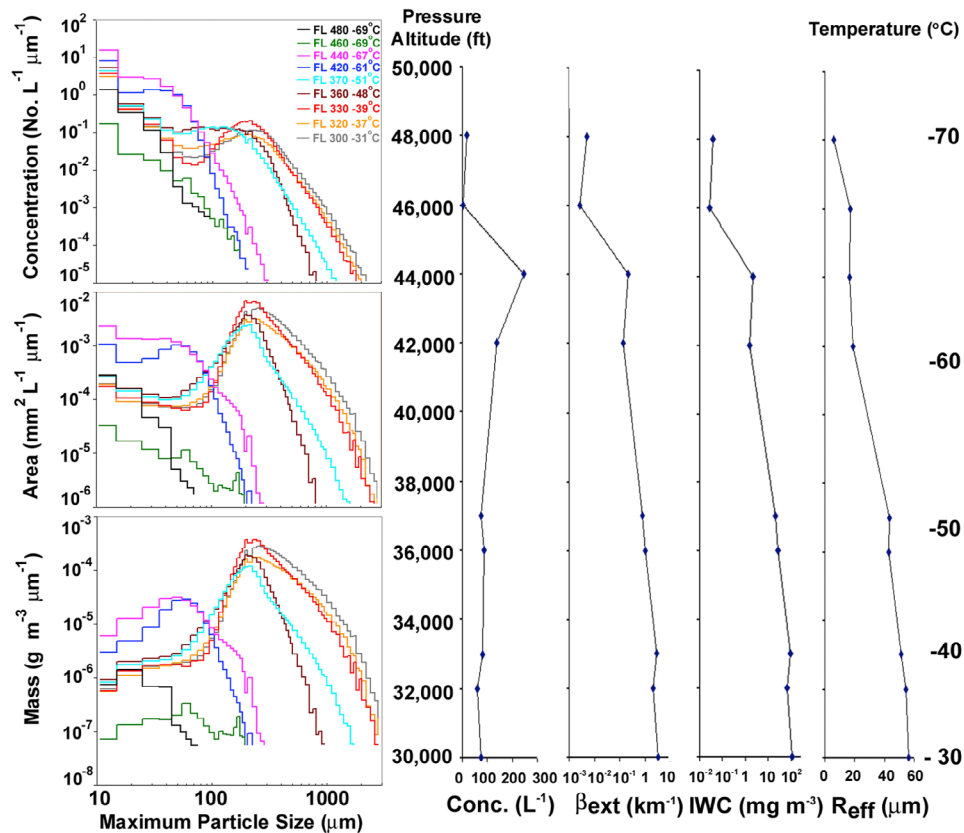
Figure 11. (left) Particle size distributions averaged over horizontal legs from WB-57F, 12.9 km 14.6 km (FL420 to FL480) and DC-8, 9.2 km to 11.3 km (FL300 to FL370) measurements in aged cirrus. (right) Vertical profiles of bulk properties from averaged size distributions at each flight level. Conc. is total particle concentration, β_{exr} is extinction coefficient, IWC is ice water content and R_{eff} is effective particle radius. See text for further discussion.

decreases from 56.1 to 43.2 μm and β_{ext} decreases from 3.3 to 0.78 km^{-1}. The optical depth of the cloud region between 14.6 km (FL480) and 12.8 km (FL420) is about 0.1, compared with an optical depth of about 4 for the cloud region between 11.3 km (FL370) and 9.2 km (FL300). The decrease in cloud particle size is similar to measurements shown by *McFarquhar and Heymsfield* [1996] in the region between 12.8 km (FL420) and 13.7 km (FL450). However, their measurements used a 2D-C probe, which has a time response slower than the CIP (see Figure 5), which suggests that the measurements of small (<~150 μm) ice particles reported by *McFarquhar and Heymsfield* [1996] were actually larger particles that were under sized due to slow time response and depth of field limitations [*Lawson et al.*, 2006a].

[29] Rosette shapes were seldom observed in aged cirrus, suggesting that in situ particle growth was not predominant in aged cirrus. However, our dataset is not a statistically significant sample of aged cirrus in the tropics. *Connolly et al.* [2005] found that rosettes were observed in anvils downwind of the main convection only after the particles had been advected a few hundred kilometers into a favorable growth regime. Aged anvil cirrus were not studied by the DC-8 down to lower levels in the atmosphere, so there are no in situ measurements to determine if these clouds rained at the ocean surface.

3.3. Convective Turrets

[30] Some of the updraft velocities in the vigorous portions of convective turrets were exceptionally high. For example, as shown in Figure 12, the updraft in the TC4 turret observed on 24 July 2007 reached a peak velocity of +20 m s^{-1} at 11 km (FL360, T = −47°C). The cloud particles in the upshear portion of the vigorous updrafts are mostly small frozen quasi-spherical particles and millimeter-sized graupel particles (Figure 12). In contrast, the downshear portion contains zero or negative vertical velocities and the larger particles are less-dense aggregates. *Cooper and Lawson* [1984] observed that graupel particles were prevalent in convection when the LWC exceeded about 1 g m^{-3}, while aggregates were more frequent in convection with LWC <~0.5 g m^{-3}. Observations in TC4 convection were conducted above the level of homogeneous freezing (i.e., <−40°C), so LWC measurements are not available. The particle concentrations were very high in both TC4 and NAMMA convective turrets, averaging about 10 cm^{-3} (Table 3) with a peak value of 32 cm^{-3} in the TC4 turret on 24 July. The high, small-ice concentration is likely the result of homogenous freezing of cloud drops in the vigorous updraft. It is important to note again that the 2D-S measurements have been corrected from shattering effects.
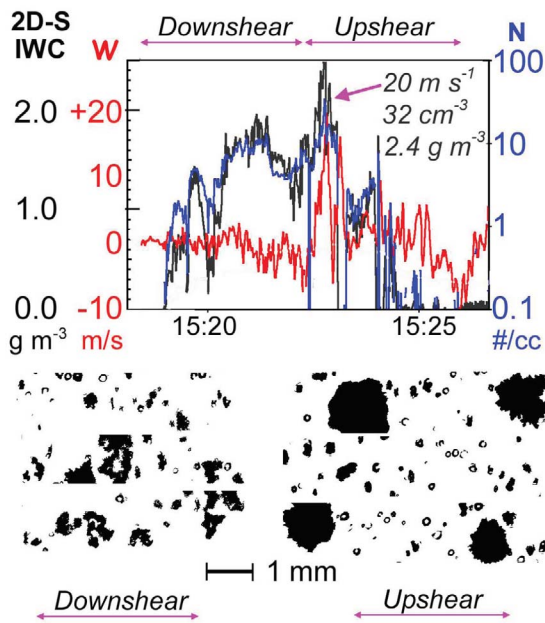
Figure 12. Example of (top) time series of IWC, vertical air velocity (w) and particle concentration (N) in the downshear and upshear regions of a vigorous TC4 updraft investigated on 24 July 2007. (bottom) Examples of 2D-S particle images.

[31] Figure 13 shows PSDs for a step-down descent through a turret investigated on 20 August 2006 during NAMMA. The PSDs in Figure 13 correspond with the examples of 2D-S particle images shown in Figure 4. Two features are particularly noticeable in Figure 13. Small (10 to 100 μm) particles are observed in high concentrations on the passes at 2.4 km (8,000 ft), 4.9 km (16,000 ft) and 6.4 km (FL210). CPI images indicate that the small particles at 2.4 km (8,000 ft) are all cloud drops that have activated and grown in the updraft. At 4.9 km (16,000 ft) the concentration of 10 to 100 μm particles have decreased, likely due to entrainment, dilution and evaporation in the updraft. At 6.4 km (FL210) most of the small particles are still liquid and the PSD is similar to that seen at 16,000 ft. However, a noticeable difference occurs above 6.4 km (FL210, T = −11°C) where the images all appear to be ice particles, which agrees with the observations of *Stith et al.* [2002]. Noticeable in the present study is the decrease in the concentration of particles from 10 to 100 μm and the increase in particle concentration from 100 to 400 μm above 6.4 km (FL210), which corresponds to T = −12°C. This has been explained in the discussion in the previous section; however, this is the first time this has been observed using a single cloud particle probe capable of covering the whole size range from 10 to 1000 μm. Previously, measurements have been pieced together using the FSSP (3 to 45 μm) and the 2D-C, which ostensibly measured particles from 25 to 800 μm, but has been found to have significant errors sizing particles with diameters less than about 125 μm [*Strapp et al.*, 2001; *Lawson et al.*, 2006a]. Measurements of particle development in updrafts using 2D-S data may be valuable for validating liquid to ice phase conversion rates in cloud resolving models.

[32] Another striking feature seen in Figure 13 is the dearth of drops from 40 to 100 μm in the rain shaft penetrated at 1200 ft. *Baker et al.* [2009a] analyzed 237 penetrations of rain shafts penetrated during the RICO project and reported a very similar PSD shape to that seen in Figure 13. The warm rain process was predominate in the much shallower RICO clouds, but maximum raindrop diameters were 2 to 3 mm, similar to the rain shaft PSD shown in Figure 13.

[33] The value of volumetric extinction coefficient in the turrets is about 80 km^{-1} and IWC is about 2 g m^{-3} (Table 3). These values are high, especially in maritime, Tropical convection, but not unprecedented. Relatively high IWC values, from 2 to 3 g m^{-3}, have been reported in the tops of anvils investigated in the Central Pacific and in Montana [*Lawson et al.*, 1998a]. Regions with high IWC in convective anvils are now thought to be responsible for several engine failures on commercial jet airliners [*Lawson et al.*, 1998a; *Pazstor*, 2008].

4. Radiative Properties of TC4 and NAMMA Clouds

[34] Most treatments of the radiative properties of clouds are based on numerical models that incorporate an assumed particle size distribution, usually expressed as an exponential, gamma or double gamma distribution [*Mitchell et al.*, 2010]. In the past, when actual measurements have been used to compute cloud radiative properties [e.g., *Ivanova et al.*, 2001], the particle size distribution has been pieced together using an FSSP probe (3 to 45 μm) that is contaminated with shattered artifacts [*Field et al.*, 2003] and a 2D-C probe that is insensitive to particles smaller than about 100 μm. The development of the 2D-S probe and its improved particle measurement characteristics (i.e., accurate particle sizing from 10 μm to mm-sized particles), provides motivation to re-examine the radiative properties of tropical clouds. Here we use actual cloud particle measurements from TC4 and NAMMA to compute asymmetry parameter, extinction coefficient and single scattering albedo, which in turn are used to compute radiative heating profiles. Heating rate profiles are compared for the four types of cloud systems described in section 3. We compare the heating rate profiles from using the actual cloud particle measurements with profiles using parameterized optical properties typically used in GCM radiative transfer codes. Finally, a simple parameterization, based on in situ measurements that pro-
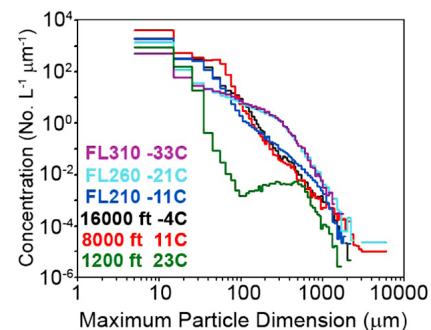
Figure 13. Particle size distributions from step-down penetrations of a NAMMA convective turret investigated on 20 August 2006.
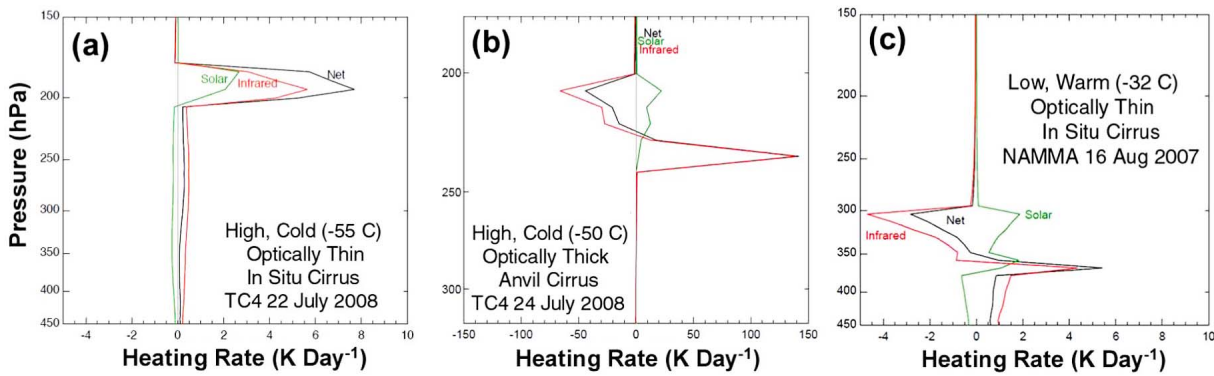
Figure 14. Vertical profiles of solar (green), infrared (red) and net (black) radiative heating rates computed using 2D-S data collected by the DC-8 in the various cloud types shown. Details of how the measurements are used to compute optical properties and heating rates are described in the text. (Note that the x-axis scale is different for the optically thicker cases.)

vide particle area as a function of particle mass, is suggested as a computationally efficient tool for use in radiative transfer codes.

4.1. Computing Optical Properties From Actual Measurements

[35] *Mitchell* [2000, 2002] and *Mitchell et al.* [1996, 2006] describe a method for computing optical properties of water drops and ice particles from their size distributions and shapes. The method is applicable to both solar and terrestrial radiation, and is accurate at a given wavelength within 15% when compared against Finite Difference Time Domain calculations. The modified anomalous diffraction approximation (MADA) uses the volume (V) and projected area (A) of a cloud particle to compute extinction and absorption coefficients via an analytical or numerical integration over the size distributions, from which extinction coefficient and single scattering albedo are determined. However, MADA does not compute scattering phase function, from which asymmetry parameter (g) can be computed. We use particle size distribution, shape and wavelength band and a technique described by *Mitchell et al.* [1996] to compute g for solar radiation, and a parameterization described by *Yang et al.* [2005] that gives g for long-wave radiation. Note that g for long wave radiation is relatively insensitive to cirrus particle shape since most radiation is forward scattered. Extinction coefficient, single scattering albedo and g are then used as inputs for the *Toon et al.* [1989] two-stream radiative transfer model.

[36] As discussed in Section 3, the 2D-S provides good microphysical measurements of particle V and A. The CPI provided good images of particle shape for particles less than about 300 μm in size on the DC-8 (due to sampling location), and for all sizes on the WB-57F. These microphysical data are input into the MADA code and used to compute single-scattering albedo (SSA), extinction coefficient and g from TC4 and NAMMA data. Particle shape attributes are primarily defined by V and A PSDs, with secondary information provided by shape recipes (i.e., percentage of each shape), which are used in the calculation of asymmetry parameter for solar radiation. Shape recipes are also used to estimate the absorption/extinction contribution from wave resonance (i.e. photon tunneling), which is a function of wavelength, particle size and shape. Optical properties were computed from DC-8 microphysical data collected during all horizontal legs flown at constant altitude through the four cloud types described in Section 3.

4.2. Radiative Heating Profiles in TC4 and NAMMA Clouds

[37] The *Toon et al.* [1989] radiative transfer model was run using as inputs the optical properties (extinction, asymmetry parameter and single scattering albedo) computed using the Mitchell MADA code. The *Toon et al.* [1989] model extends the solution of a generalized two-stream approximation for radiative transfer in homogeneous multiple scattering atmospheres to vertically inhomogeneous atmospheres. The model is numerically stable, computationally efficient and is accurate to better than 10%.

[38] Figure 14 shows a comparison of heating profiles for two high, cold, geometrically thin clouds and one lower, warmer, geometrically thin cloud. The profile in Figure 14a is for optically thin in situ cirrus and the profile in Figure 14b is for optically thick anvil cirrus. The defining difference is that the in situ cirrus shows a net heating throughout the cloud, while the optically thick anvil cirrus shows heating at cloud base and cooling at cloud top (also note that the magnitude of both heating and cooling is much greater in the anvil cirrus). In the case of the anvil cirrus, upwelling infrared radiation (IR) is fully absorbed in the optically thick lower level of cloud. Therefore, the net IR radiation from the upper portion of cloud is directed upwards toward space. In contrast, upwelling IR warming from below penetrates throughout the depth of the optically thin in situ cirrus and overwhelms IR emissive loss to space. Upper level heating profiles from high, cold, thin cirrus is thought to balance adiabatic cooling driven by vertical motions in the upper troposphere and may contribute to troposphere/stratosphere transport [*Corti et al.*, 2006]. The heating profile in Figure 14c is for a lower, warmer optically thin in situ cirrus cloud compared to the higher, colder cirrus in Figure 14a. The reason for the difference in heating profiles is that the lower, warmer in situ cirrus cloud absorbs and emits (proportional to the fourth power of absolute temperature) at a much warmer temperature, so that the cloud more effectively emits upwelling IR radiation. Note, however, that although
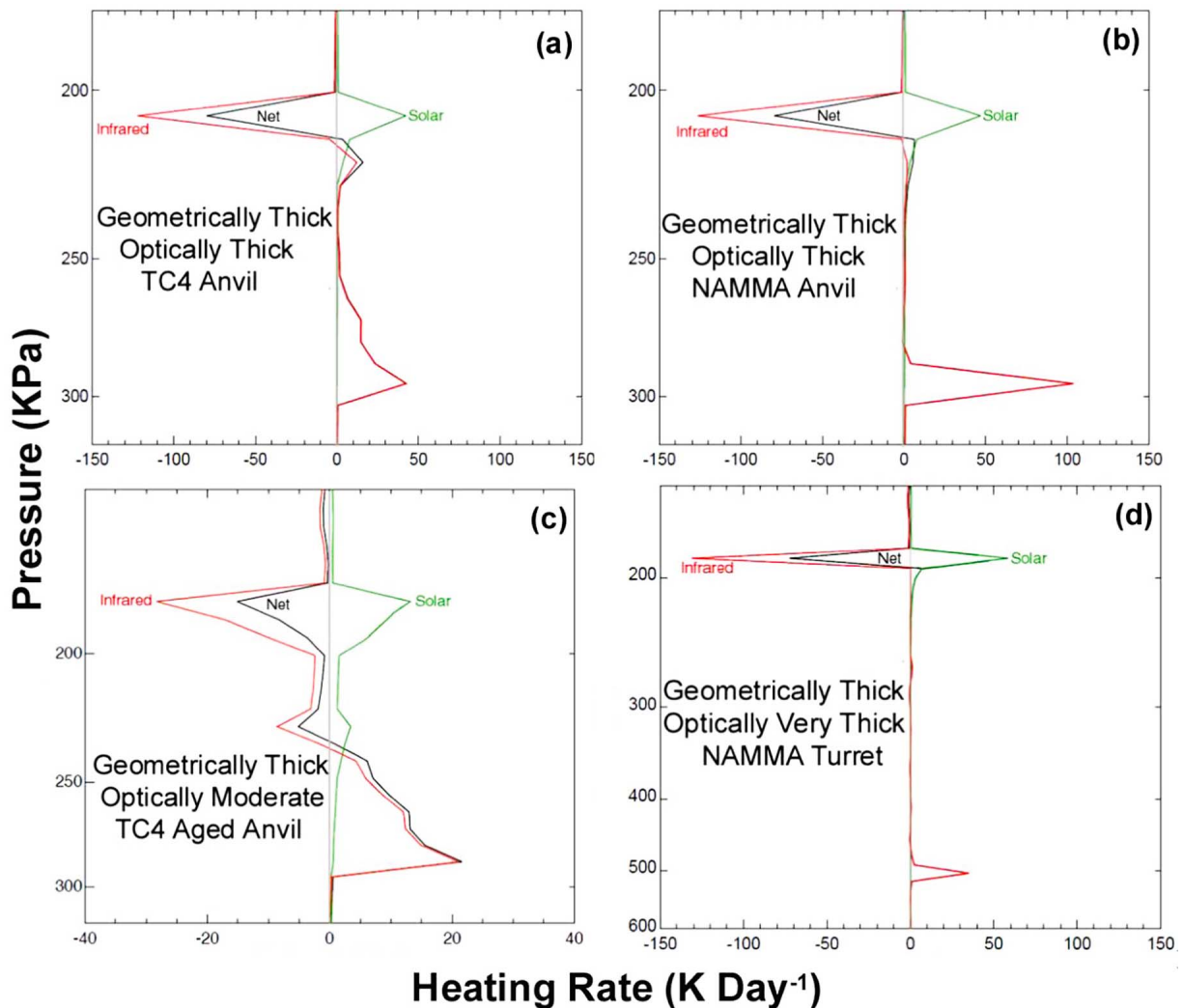
Figure 15. Same as in Figure 14 but for different cloud types. (Note that the x-axis scale is different for the optically thicker cases.)

the warmer in situ cirrus cloud (Figure 14c) has the same heating profile as the higher, colder anvil cloud (Figure 14b), the absolute magnitude of heating and cooling is much less in the optically thinner cloud.

[39] Figure 15 shows a comparison of four heating profiles from three cloud types. The profiles in Figures 15a and 15b are geometrically thick, optically thick anvils from TC4 and NAMMA. Both heating profiles are similar, which is expected since the microphysical properties of TC4 and NAMMA anvil clouds are very similar. The NAMMA anvil has a sharper IR absorption profile near cloud base due to a slightly higher mass concentration at this level. The heating profile in Figure 15c is for aged anvil cirrus. Even though this cloud is geometrically as thick as the fresh anvils, it is optically much thinner, which is reflected in the heating profile. Upwelling IR radiation is not as rapidly absorbed at cloud base as in the fresh anvils, outgoing IR radiates from deeper in the cloud and incoming solar radiation penetrates deeper into the cloud. The heating profile for turrets in Figure 15c is for the geometrically and optically thickest

cloud. Both IR and solar incoming radiation are absorbed within the first few hundreds of meters, and outgoing IR radiation is emitted from the first few hundred meters.

[40] To reemphasize, the heating profiles computed in Figures 14 and 15 were computed using actual 2D-S measurements of projected surface area. Generally, numerical cloud models compute mass, assume a particle size distribution, habit and ice particle geometry [e.g., *Auer and Veal*, 1970] to compute optical properties using ray tracing. However, often the assumed ice crystal dimensions are not representative of rimed and aggregated ice particles found in ice clouds, such as the Tropical cirrus and anvils investigated in TC4 and NAMMA. *Baker and Lawson* [2006a] developed an equation to compute particle mass from projected area based on the analysis of photographed and melted ice crystals:

$$M = 0.155A^{1.218}, \qquad (1)$$

where M is particle mass in mg and A is particle-projected area in mm. The very good comparison of 2D-S and CVI
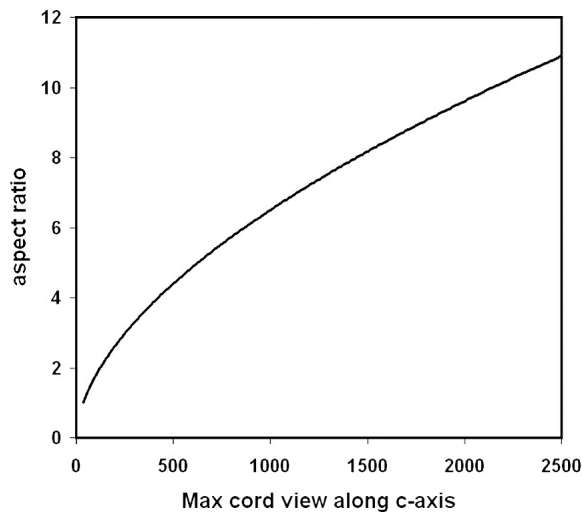
Figure 16. Plot of equation (2), which shows the relationship between aspect ratio and ice particle maximum dimension for a hexagonal crystal (plotted as max cord view along the c-axis).

mass measurements shown in Figure 6 gives strong support for the applicability of (1) to the types of ice particles measured by the 2D-S in Tropical cirrus and anvil clouds. A relationship for the aspect ratio of a plate as a function of particle maximum dimension can be determined by applying hexagonal plate geometry. This is accomplished by substituting for the area of the basal face of a plate, $A_P = \frac{3}{8}\sqrt{3}\,L^2$, for A in (1), where L is maximum dimension across the basal face, and setting the result equal to the mass of a hexagonal plate, or

$$0.155 \left(\frac{3}{8}\sqrt{3}\,L^2 \right)^{1.218} = \frac{\rho_i L}{R_A} \left(\frac{3}{8}\sqrt{3}\,L^2 \right)$$

Solving for aspect ratio gives

$$R_A = 6.499\, L^{0.564}, \tag{2}$$

where $\rho_i = 0.916$ is the density of ice. Equation (2) is plotted in Figure 16. As expected, the plot shows an increasing aspect ratio with increasing size, with a 1 mm ice particle having an aspect ratio of 6.5:1. This is comparable to aspect ratios for large aggregates, which have been estimated to have aspect ratios of about 3:1 to 8:1 [e.g., *Lawson et al.*, 1998b]. However, this is considerably different than the 50:1 aspect ratio of (pristine) 1 mm plate crystals observed by *Auer and Veal* [1970] in a mountain cap cloud. The measurements by Auer and Veal were carefully done and are certainly accurate, but these measurements are for pristine, vapor grown plates, not rimed aggregates.

[41] The development presented above suggests an alternative method for computing optical properties in numerical models of Tropical cirrus and anvil clouds. Equation (1) can be inverted to give

$$A = 4.621\, M^{0.821}, \tag{3}$$

which can be used, along with mass and particle type in the *Mitchell* [2002] MADA code to compute single-scattering albedo, extinction and asymmetry parameter.

5. Summary

[42] Measurements from the relatively new 2D-S probe are used to investigate the microphysical and radiative properties of several types of Tropical clouds, including cirrus formed in situ, convective turrets, anvil cirrus and aged anvil cirrus. The observations were conducted by the NASA DC-8 (with some additional measurements from the NASA WB-57) research aircraft during the 2006 NAMMA and 2007 TC4 field campaigns. The use of the 2D-S data are significant here because these are the first measurements from a single cloud particle probe that have reliably covered the size range from about 10 μm to 3 mm. Previous investigations have typically blended together measurements from two instruments, a scattering instrument, the FSSP (or CAS) and an imaging probe, the 2D-C (or CIP). The FSSP and CAS probes are known to overestimate the number of small particles due to shattering of large ice on their inlets [*Field et al.*, 2003; *Jensen et al.*, 2009] and the 2D-C and CIP have significant sizing and counting errors for particles with sizes less than about 200 μm at the airspeed of jet aircraft [*Korolev et al.*, 1998; *Strapp et al.*, 2001; *Lawson et al.*, 2006a]. In contrast, the 2D-S probe has been shown to accurately image particles as small as 10 μm at speeds up to 233 m s^{-1} [*Lawson et al.*, 2006a, 2008; *Jensen et al.*, 2009; *Baker et al.*, 2009a, 2009b].

[43] Investigations of in situ cirrus during both the NAMMA and TC4 field campaigns were limited, but adequate to show that recognizable particle habits were very similar to the rosette shapes commonly seen in mid-latitude cirrus [e.g., *Heymsfield et al.*, 2002; *Lawson et al.*, 2006b]. Also, average extinction coefficient (0.5 km^{-1} in TC4, 0.67 km^{-1} in NAMMA, 0.92 km^{-1} in mid-latitude cirrus) and IWC (0.011 g m^{-3} in TC4, 0.019 g m^{-3} in NAMMA, 0.013 g m^{-3} in mid-latitude cirrus) are of the same order in all three locations. However, average total particle concentration was much lower in the Tropical in situ cirrus, 198 L^{-1} in TC4 and 37 L^{-1} in NAMMA, compared with 846 L^{-1} observed by *Lawson et al.* [2006b] in mid-latitude cirrus. The measurements of small particles reported by *Lawson et al.* [2006b] were largely based on an FSSP, and were likely contaminated by shattered crystals. The shattering probably contributed to the higher values of extinction coefficient reported in the mid-latitude cirrus.

[44] The particle shapes in convective turrets, fresh and aged anvils were distinctly different in that there were no rosette shapes, with the rare exception of occasional rosette shapes in aged anvil cirrus far downwind of convection. It is likely that these rosette shaped ice crystals formed in regions of higher humidity. Extinction coefficient and IWC was dominated by particles in the size range from 100 to 400 μm in both turrets and anvils. Based on data collected in the Tropical storms discussed here, most cloud drops tend to nucleate in updrafts by the time they reach the -12°C level (with the exception of extremely vigorous updrafts) and grow to ice particles with sizes of a few hundred microns by the time they are ejected into the anvil. The rare drops that nucleate lower in the updraft become graupel particles and

fall out of the updraft. The drops that do not nucleate heterogeneously, or are converted to ice via diffusional growth or accretion, freeze homogeneously and are ejected into the anvil. Overall, this scenario favors development of ice particles that end up in the 100 to 400 μm size range. In the anvil the smallest and largest particles "disappear" more rapidly than the intermediate size particles. That is, the very small particles sublimate or aggregate with other ice particles. The largest (millimeter size) particles sediment rapidly and fall out of the anvil. The intermediate size (100 to 400 μm) particles either aggregate into larger sizes and fall out rapidly, or remain in the anvil as they slowly sediment or sublimate. Again, this process favors the longevity of the intermediate size particles, which are typically observed in TC4 and NAMMA anvils.

[45] The 2D-S measurements indicate that particle number concentration was typically about 10 cm^{-3} in both NAMMA and TC4 convective turrets, being slightly higher in TC4 clouds. Extinction coefficient and IWC were one the order of 50 to 60 km^{-1} and 1.5 g m^{-3}, respectively. One exceptionally vigorous turret investigated in TC4 at 11.3 km (FL370, T = −47°C) had a number concentration of 32 cm^{-3}, a peak updraft velocity of 20 m s^{-1} and IWC of 2.2 g m^{-3}.

[46] A rain shaft investigated in NAMMA showed a dearth of drops in the size range from 20 to 100 μm, while measurements above this level showed high concentrations of drops and ice particles in this size range. Again, these are unique measurements because all previous instruments were either affected by splashing of drops on tips and inlets and/or incapable of measuring drops in this size range. Interestingly, *Baker et al.* [2009a] analyzed 237 RICO rain shafts and found a similar result, virtually no drops in the 20 to 100 μm size range. They concluded that the drops observed from about 10 to 30 μm were deliquesced aerosols.

[47] The 2D-S area and mass size distribution measurement were fed into the *Mitchell* [2002] MADA code to compute optical properties: extinction, single-scattering albedo and asymmetry parameter. The optical properties were then ingested in the *Toon et al.* [1989] two-stream radiative transfer model to compute cloud-heating profiles for in situ cirrus, convective turrets, fresh and aged anvil cirrus. The power law relationship between mass and area size distribution can be used along with the MADA code as a parameterization in models of radiative transfer. These results showing microphysical and radiative properties of in situ cirrus, anvil cirrus and convective turrets can be compared directly with output from cloud resolving and radiative transfer models.

References

Auer, A. H., Jr., and D. L. Veal (1970), The dimensions of ice crystals in natural clouds, *J. Atmos. Sci.*, *27*, 919–926, doi:10.1175/1520-0469(1970)027<0919:TDOICI>2.0.CO;2.

Baker, B. A., and R. P. Lawson (2006a), Improvement in determination of ice water content from two-dimensional particle imagery: Part I: Image to mass relationships, *J. Appl. Meteorol.*, *45*, 1282–1290, doi:10.1175/JAM2398.1.

Baker, B. A., and R. P. Lawson (2006b), In situ observations of the microphysical properties of wave, cirrus and anvil clouds. Part 1: Wave clouds, *J. Atmos. Sci.*, *63*, 3160–3185, doi:10.1175/JAS3802.1.

Baker, B. A., A. Korolev, R. P. Lawson, D. O'Connor, and Q. Mo (2009a), Drop size distributions and the lack of small drops in RICO rain shafts, *J. Appl. Meteorol.*, *48*, 616–623, doi:10.1175/2008JAMC1934.1.

Baker, B., Q. Mo, R. P. Lawson, D. O'Conner, and A. Korolev (2009b), The effects of precipitation on cloud droplet measurement devices, *J. Atmos. Oceanic Technol.*, *26*, 1404–1409, doi:10.1175/2009JTECHA1191.1.

Baumgardner, D., J. E. Dye, R. G. Knollenberg, and B. W. Gandrud (1992), Interpretation of measurements made by the FSSP-300X during the Airborne Arctic Stratospheric Expedition, *J. Geophys. Res.*, *97*(D8), 8035–8046.

Baumgardner, D., H. Jonsson, W. Dawson, D. O'Connor, and R. Newton (2001), The cloud, aerosol and precipitation spectrometer (CAPS): A new instrument for cloud investigations, *Atmos. Res.*, *59-60*, 251–264, doi:10.1016/S0169-8095(01)00119-3.

Connolly, P. J., C. P. R. Saunders, M. W. Gallagher, K. N. Bower, M. J. Flynn, T. W. Choularton, J. Whiteway, and R. P. Lawson (2005), Aircraft observations of the influence of electric fields on the aggregation of ice crystals, *Q. J. R. Meteorol. Soc.*, *131*, 1695–1712, doi:10.1256/qj.03.217.

Cooper, W. A. (1978), *Cloud Physics Investigations by the University of Wyoming in HIPLEX 1977*, 320 pp., U.S. Bur. of Reclamation, Washington, D. C.

Cooper, W. A., and R. P. Lawson (1984), Physical interpretation of results from the HIPLEX-1 Experiment, *J. Appl. Meteorol.*, *23*, 523–540, doi:10.1175/1520-0450(1984)023<0523:PIORFT>2.0.CO;2.

Corti, T., B. P. Luo, Q. Fu, H. Vömel, and T. Peter (2006), The impact of cirrus clouds on tropical troposphere-to-stratosphere transport, *Atmos. Chem. Phys.*, *6*, 2539–2547, doi:10.5194/acp-6-2539-2006.

Davis, S. M., L. M. Avallone, B. H. Kahn, K. G. Meyer, and D. Baumgardner (2009), Comparison of airborne in situ measurements and Moderate Resolution Imaging Spectroradiometer (MODIS) retrievals of cirrus cloud optical and microphysical properties during the Midlatitude Cirrus Experiment (MidCiX), *J. Geophys. Res.*, *114*, D02203, doi:10.1029/2008JD010284.

Field, P. R., R. Wood, P. R. A. Brown, P. H. Kaye, E. Hirst, and R. Greenaway (2003), Ice particle interarrival times measured with a fast FSSP, *J. Atmos. Oceanic Technol.*, *20*, 249–261, doi:10.1175/1520-0426(2003)020<0249:IPITMW>2.0.CO;2.

Field, P. R., A. J. Heymsfield, and A. Bansemer (2006), Shattering and particle interarrival times measured by optical array probes in ice clouds, *J. Atmos. Oceanic Technol.*, *23*, 1357–1371, doi:10.1175/JTECH1922.1.

Fridlind, A. M., et al. (2004), Evidence for the predominance of mid-tropospheric aerosols as subtropical anvil nuclei, *Science*, *304*, 718–722, doi:10.1126/science.1094947.

Garrett, T. J., H. Gerber, D. G. Baumgardner, C. H. Twohy, and E. M. Weinstock (2003), Small, highly reflective ice crystals in low-latitude cirrus, *Geophys. Res. Lett.*, *30*(21), 2132, doi:10.1029/2003GL018153.

Garrett, T. J., et al. (2005), Evolution of a Florida cirrus anvil, *J. Atmos. Sci.*, *62*, 2352–2372, doi:10.1175/JAS3495.1.

Gayet, J.-F., F. Auriol, A. Minikin, J. Ström, M. Seifert, R. Krejci, A. Petzold, G. Febvre, and U. Schumann (2002), Quantitative measurement of the microphysical and optical properties of cirrus clouds with four different in-situ probes: Evidence of small ice crystals, *Geophys. Res. Lett.*, *29*(24), 2230, doi:10.1029/2001GL014342.

Griffith, K. T., S. K. Cox, and R. G. Knollenberg (1980), Infrared radiative properties of tropical cirrus clouds inferred from aircraft measurements, *J. Atmos. Sci.*, *37*, 1077–1087, doi:10.1175/1520-0469(1980)037<1077:IRPOTC>2.0.CO;2.

Heymsfield, A. J. (2007), On measurements of small ice particles in clouds, *Geophys. Res. Lett.*, *34*, L23812, doi:10.1029/2007GL030951.

Heymsfield, A. J., S. Lewis, A. Bansemer, J. Iaquinta, L. M. Miloshevich, M. Kajikawa, C. Twohy, and M. R. Poellot (2002), A general approach for deriving the properties of cirrus and stratiform ice cloud particles, *J. Atmos. Sci.*, *59*, 3–29, doi:10.1175/1520-0469(2002)059<0003:AGAFDT>2.0.CO;2.

Ivanova, D., D. L. Mitchell, W. P. Arnott, and M. Poellot (2001), A GCM parameterization for bimodal size spectra and ice mass removal rates in mid-latitude cirrus clouds, *Atmos. Res.*, *59–60*, 89–113, doi:10.1016/S0169-8095(01)00111-9.

Jensen, E. J., S. Kinne, and O. B. Toon (1994), Tropical cirrus cloud radiative forcing: Sensitivity studies, *Geophys. Res. Lett.*, *21*(18), 2023–2026, doi:10.1029/94GL01358.

Jensen, E. J., et al. (2009), On the importance of small ice crystals in tropical anvil cirrus, *Atmos. Chem. Phys. Discuss.*, 9, 5321–5370.

Kärcher, B., and J. Ström (2003), The roles of dynamical variability and aerosols in cirrus cloud formation, *Atmos. Chem. Phys.*, 3, 823–838, doi:10.5194/acp-3-823-2003.

Knollenberg, R. G. (1981), Techniques for probing cloud microstructure, in *Clouds, Their Formation, Optical Properties, and Effects*, edited by P.V. Hobbs, pp. 15-91, Academic, San Diego, Calif.

Knollenberg, R. G., A. J. Dascher, and D. Huffman (1982), Measurements of the aerosol and ice crystal populations in tropical stratospheric cumulonimbus anvils, *Geophys. Res. Lett.*, 9(6), 613–616, doi:10.1029/GL009i006p00613.

Knollenberg, R. G., K. Kelly, and J. C. Wilson (1993), Measurements of high number densities of ice crystals in the tops of tropical cumulonimbus, *J. Geophys. Res.*, 98(D5), 8639–8664, doi:10.1029/92JD02525.

Korolev, A. V., and G. A. Isaac (2005), Shattering during sampling by OAPs and HVPS. Part I: Snow particles, *J. Atmos. Oceanic Technol.*, 22, 528–542, doi:10.1175/JTECH1720.1.

Korolev, A. V., J. W. Strapp, and G. A. Isaac (1998), Evaluation of the accuracy of PMS optical array probes, *J. Atmos. Oceanic Technol.*, 15, 708–720, doi:10.1175/1520-0426(1998)015<0708:EOTAOP>2.0.CO;2.

Korolev, A. V., G. A. Isaac, and J. Hallett (1999), Ice particle habits in Arctic clouds, *Geophys. Res. Lett.*, 26(9), 1299–1302, doi:10.1029/1999GL900232.

Lawson, R. P., L. J. Angus, and A. J. Heymsfield (1998a), Cloud particle measurements in thunderstorm anvils and possible weather threat to aviation, *J. Aircr.*, 35, 113–121, doi:10.2514/2.2268.

Lawson, R. P., R. E. Stewart, and L. J. Angus (1998b), Observations and numerical simulations of the origin and development of very large snowflakes, *J. Atmos. Sci.*, 55, 3209–3229, doi:10.1175/1520-0469(1998)055<3209:OANSOT>2.0.CO;2.

Lawson, R. P., D. O'Connor, P. Zmarzly, K. Weaver, B. A. Baker, Q. Mo, and H. Jonsson (2006a), The 2D-S (Stereo) probe: Design and preliminary tests of a new airborne, high-speed, high-resolution imaging probe, *J. Atmos. Oceanic Technol.*, 23, 1462–1477, doi:10.1175/JTECH1927.1.

Lawson, R. P., B. A. Baker, B. Pilson, and Q. Mo (2006b), In Situ observations of the microphysical properties of wave, cirrus and anvil clouds. Part II: Cirrus clouds, *J. Atmos. Sci.*, 63, 3186–3203, doi:10.1175/JAS3803.1.

Lawson, R. P., B. Pilson, B. Baker, Q. Mo, E. Jensen, L. Pfister, and P. Bui (2008), Aircraft measurements of microphysical properties of subvisible cirrus in the tropical tropopause layer, *Atmos. Chem. Phys.*, 8, 1609–1620, doi:10.5194/acp-8-1609-2008.

McFarquhar, G. M., and A. J. Heymsfield (1996), Microphysical characteristics of three anvils sampled during the Central Equatorial Pacific Experiment, *J. Atmos. Sci.*, 53, 2401–2423, doi:10.1175/1520-0469(1996)053<2401:MCOTAS>2.0.CO;2.

McFarquhar, G. M., et al. (2010), Indirect and Semi-Direct Aerosol Campaign (ISDAC): The impact of Arctic aerosols on clouds, *Bull. Am. Meteorol. Soc.*, in press.

Mishchenko, M. I., W. B. Rossow, A. Macke, and A. A. Lacis (1996), Sensitivity of cirrus cloud albedo, bidirectional reflectance, and optical thickness retrieval accuracy to ice-particle shape, *J. Geophys. Res.*, 101(D12), 16,973–16,985, doi:10.1029/96JD01155.

Mitchell, D. L. (2000), Parameterization of the Mie extinction and absorption coefficients for water clouds, *J. Atmos. Sci.*, 57, 1311–1326, doi:10.1175/1520-0469(2000)057<1311:POTMEA>2.0.CO;2.

Mitchell, D. L. (2002), Effective diameter in radiation transfer: General definition, applications and limitations, *J. Atmos. Sci.*, 59, 2330–2346, doi:10.1175/1520-0469(2002)059<2330:EDIRTG>2.0.CO;2.

Mitchell, D. L., A. Macke, and Y. Liu (1996), Modeling cirrus clouds. Part II: Treatment of radiative properties, *J. Atmos. Sci.*, 53, 2967–2988, doi:10.1175/1520-0469(1996)053<2967:MCCPIT>2.0.CO;2.

Mitchell, D. L., A. J. Baran, W. P. Arnott, and C. Schmitt (2006), Testing and comparing the modified anomalous diffraction approximation, *J. Atmos. Sci.*, 63, 2948–2962, doi:10.1175/JAS3775.1.

Mitchell, D. L., P. Rasch, D. Ivanova, G. McFarquhar, and T. Nousiainen (2008), Impact of small ice crystal assumptions on ice sedimentation rates in cirrus clouds and GCM simulations, *Geophys. Res. Lett.*, 35, L09806, doi:10.1029/2008GL033552.

Mitchell, D. L., R. P. d'Entremont, and R. P. Lawson (2010), Inferring cirrus size distributions through satellite remote sensing and microphysical databases, *J. Atmos. Sci.*, 67, 1106–1125, doi:10.1175/2009JAS3150.1.

Pazstor, A. (2008), Airline regulators grapple with engine-shutdown peril, *Wall Street J.*, 7 April.

Sanderson, B. M., C. Piani, W. J. Ingram, D. A. Stone, and M. R. Allen (2008), Towards constraining climate sensitivity by linear analysis of feedback patterns in thousands of perturbed-physics GCM simulations, *Clim. Dyn.*, 30, 175-190, doi:10.1007/s00382007-0280.

Sinha, A., and K. P. Shine (1994), A one-dimensional study of possible cirrus cloud feedbacks, *J. Clim.*, 7, 158–173, doi:10.1175/1520-0442(1994)007<0158:AODSOP>2.0.CO;2.

Stackhouse, P. W. J., and G. L. Stephens (1991), A theoretical and observational study of the radiative properties of cirrus: Results from FIRE 1986, *J. Atmos. Sci.*, 48, 2044–2059, doi:10.1175/1520-0469(1991)048<2044:ATAOSO>2.0.CO;2.

Stephens, G. L., S.-C. Tsay, P. W. Stackhouse, and P. J. Flatau (1990), The relevance of the microphysical and radiative properties of cirrus clouds to climate and climatic feedback, *J. Atmos. Sci.*, 47, 1742–1753, doi:10.1175/1520-0469(1990)047<1742:TROTMA>2.0.CO;2.

Stith, J. L., J. E. Dye, A. Bansemer, A. J. Heymsfield, C. A. Grainger, W. A. Peterson, and R. Cifelli (2002), Microphysical observations of tropical clouds, *J. Appl. Meteorol.*, 41, 97–117, doi:10.1175/1520-0450 (2002)041<0097:MOOTC>2.0.CO;2.

Strapp, J. W., F. Albers, A. Reuter, A. V. Korolev, U. Maixner, E. Rashke, and Z. Vukovic (2001), Laboratory measurements of the response of a PMS OAP-2DC, *J. Atmos. Oceanic Technol.*, 18, 1150–1170, doi:10.1175/1520-0426(2001)018<1150:LMOTRO>2.0.CO;2.

Tian, L., G. M. Heymsfield, A. J. Heymsfield, A. Bansemer, L. Li, C. H. Twohy, and R. C. Srivastava (2010), A study of cirrus ice particle size distribution using TC4 observations, *J. Atmos. Sci.*, 67, 195–216, doi:10.1175/2009JAS3114.1.

Toon, O. B., C. P. McKay, T. P. Ackerman, and K. Santhaman (1989), Rapid calculation of radiative heating and photodissociation rates in inhomogeneous multiple scattering atmospheres, *J. Geophys. Res.*, 94(D13), 16,287–16,301.

Toon, O. B., et al. (2010), Planning, implementation, and first results of the Tropical Composition, Cloud and Climate Coupling Experiment (TC4), *J. Geophys. Res.*, 115, D00J04, doi:10.1029/2009JD013073.

Twohy, C. H., A. J. Schanot, and W. A. Cooper (1997), Measurement of condensed water content in liquid and ice clouds using an airborne counterflow virtual impactor, *J. Atmos. Oceanic Technol.*, 14, 197–202, doi:10.1175/1520-0426(1997)014<0197:MOCWCI>2.0.CO;2.

Vizy, E. K., and K. H. Cook (2009), Tropical storm development from African easterly waves in the eastern Atlantic: A comparison of two successive waves using a regional model as part of NASA AMMA 2006, *J. Atmos. Sci.*, 66, 3313–3334, doi:10.1175/2009JAS3064.1.

Yang, P., H. Wei, H.-L. Huang, B. A. Baum, Y. X. Hu, G. W. Kattawar, M. I. Mishchenko, and Q. Fu (2005), Scattering and absorption property database for nonspherical ice particles in the near-through far-infrared spectral region, *Appl. Opt.*, 44, 5512–5523, doi:10.1364/AO.44.005512.

B. Baker, R. P. Lawson, Q. Mo, and B. Pilson, SPEC, Incorporated, 3022 Sterling Cir., Boulder, CO 80301, USA. (plawson@specinc.com)

E. Jensen, NASA Ames Research Center, Moffett Field, CA 94035, USA.

D. L. Mitchell, Desert Research Institute, University of Nevada, Reno, NV 89512, USA.